PAPER

New bioactive glass scaffolds with exceptional qualities for bone tissue regeneration: response of osteoblasts and osteoclasts

Biomedical Materials

PAPER

New bioactive glass scaffolds with exceptional qualities for bone tissue regeneration: response of osteoblasts and osteoclasts

Tia J Kowal[1], Natalie C Hahn[1], Stephanie Eider[1], Jutta Y Marzillier[1], Daniella M Fodera[1], Ukrit Thamma[2], Himanshu Jain[2,3] and Matthias M Falk[1,3]

[1] Department of Biological Sciences, Lehigh University, Bethlehem, PA 18015, United States of America
[2] Department of Materials Science and Engineering, Lehigh University, Bethlehem, PA 18015, United States of America
[3] Authors to whom any correspondence should be addressed.

E-mail: H.Jain@lehigh.edu and MFalk@lehigh.edu

RECEIVED
29 June 2017

REVISED
3 October 2017

ACCEPTED FOR PUBLICATION
16 October 2017

PUBLISHED
24 January 2018

Keywords: bioactive glass, bone tissue, osteoblast, osteoclast, tissue regeneration

Supplementary material for this article is available online

Abstract

Tissue regeneration is a significantly improved alternative to tissue replacement by implants. It requires porous bioscaffolds for the restoration of natural tissue rather than relying on bio-inactive, often metallic implants. Recently, we developed technology for fabricating novel, nano-macroporous bioactive 'tailored amorphous multi-porous (TAMP)' hard tissue scaffolds using a 70 mol% SiO_2–30 mol% CaO model composition. The TAMP silicate scaffolds, fabricated by a modified sol-gel process, have shown excellent biocompatibility via the rapid formation of hydroxyapatite in biological fluids as well as in early tests with bone forming cells. Here we report an in depth investigation of the response of MC3T3-E1 pre-osteoblast cells and bone marrow derived (BMD) osteoclasts to these TAMP scaffolds. Light and electron microscopic imaging, gene and protein expression, and enzyme activity analyses demonstrate that MC3T3-E1 pre-osteoblasts adhere, proliferate, colonize, and differentiate on and inside the bioactive TAMP scaffolds. Additionally, BMD precursor cells mature into active osteoclasts and remodel the scaffold, highlighting the exceptional qualities of this novel scaffold material for bone tissue regeneration.

1. Introduction

In the 1960s, Larry Hench developed a novel material for hard tissue regeneration called Bioglass®. His revolutionary oxide glass, composed of silica, sodium, calcium, and phosphate was found to interact with cells and to bond to bone [1]. Although, many improvements have been made to the original Bioglass® over the years (reviewed in [2]), a significant remaining drawback of Bioglass® is that it is a solid material that is not susceptible to cell penetration. We have developed a next-generation bioactive glass material termed tailored amorphous multi-porous (TAMP) that is highly porous, featuring interconnected macro- (20–200 μm diameter) and nanoporosity (2.5–50 nm), that not only allows cells to colonize the TAMP scaffolds and provide improved fluid exchange and significantly enlarged reactive surface area, but also to dissolve in biological fluids over time allowing its replacement by natural tissue [3–8]. The porosity of the TAMP creates a scaffold structure that mimics the natural structure of bone which is ideal for regenerating natural tissue [9–11]. On top of that, bioactive glass dissolution products have been shown to induce the differentiation of pre-osteoblasts into mature, calcified matrix secreting osteoblasts [12–15]. We chose TAMP scaffolds composed of 70 mol% SiO_2–30 mol% CaO for our studies because of their chemical simplicity and ease of fabrication, their bioactivity, and osteoinductive properties.

Although we have reported previously on the characteristics and use of TAMP bioactive glass scaffolds [3–8], a thorough biological *in vitro* characterization using osteoblastic and osteoclastic cells has not been performed. In contrast to studies performed by others in which bioactive glass performance was judged by adding conditioned medium (medium exposed to glass) to cells [12, 13, 15, 16], we seeded cells directly onto TAMP scaffolds without the addition of osteogenic medium for all analyses. Enzymatic, RNA, and

protein analyses demonstrate that cells quickly attach to the TAMP material through the formation of robust focal adhesions and that MC3T3-E1 cells differentiate into mature bone producing osteoblasts. Additionally, bone marrow derived (BMD) precursor cells differentiate into osteoclasts (bone degrading cells) that actively remodel the scaffolds, supporting the extraordinary qualities of this novel bioactive material for bone tissue regeneration.

2. Materials and methods

2.1. TAMP scaffold preparation

70 mol% SiO_2–30 mol% CaO TAMP scaffolds were produced using a modified sol-gel method [6]. In brief, 1.4 g polyethylene oxide was dissolved in 20 ml 0.05 N acetic acid followed by addition of 9 ml tetramethyl orthosilicate and 6.18 g $Ca(NO_3)_2$-$4H_2O$. 2.5% hydrofluoric acid (HF) was added to catalyze the gelation process and the sol was pipetted into 24-well plates to gel. The gel was allowed to set at 40 °C for 24 h before 1 N NH_4OH was added for solvent exchange (also at 40 °C) over the next 3 d. The samples were dried slowly over 3 d by increasing temperature from 24 °C to 180 °C in a controlled humidity environment, followed by sintering at 700 °C. Nanoporosity and surface area were determined using Barrett–Joyner–Halenda and Brunauer–Emmett–Teller (BET) nitrogen adsorption (ASAP 2020; Micromimetics) methods by loading 0.6 g of TAMP material into the chamber of the BET, which was evacuated and heated to 150 °C to remove moisture before analysis [17]. Additionally, mercury porosimetry was performed by Micromeritics' AutoPore IV 9500 to establish the macropore size. After sintering, the samples were polished to produce a smooth surface and then autoclaved to ensure sterility for cell culture testing. Before cells were seeded, the TAMP scaffolds were pre-incubated in phosphate buffered saline (PBS) for 3 d to allow for necessary hydration and formation of hydroxyapatite (consistent with results found by [18]).

2.2. Osteoblast culture on TAMP scaffolds

MC3T3-E1 subclone 4 mouse pre-osteoblast cells (CRL-2593) were purchased from American Type Culture Collection (ATCC, Manassas, VA). Cells were maintained using standard culture conditions at 37 °C in a 5% CO_2 atmosphere and 100% humidity in alpha-modified eagles medium without ascorbic acid (α-MEM, Gibco/Invitrogen, Grand Island, NY, Cat. No. A10490-01) supplemented with 10% fetal bovine serum (Atlanta Biologicals, Flowery Branch, GA Cat. No. S11150), 1% L-glutamine (HyClone, Logan, UT Cat. No. 25-005-C1) and 1% penicillin/streptomycin (Corning, Corning, NY Cat. No.30-001-Cl). MC3T3-E1 cells were counted using a hemocytometer and seeded onto the TAMP scaffolds placed into either 3.5 cm diameter or 24-well polystyrene tissue culture plates (Genesee, San Diego, CA Cat. #25–107) at a density of 30 000 cells cm^{-2}. To maintain cells growing on TAMP scaffolds for an extended time, ½ medium was exchanged with fresh medium every 2–3 days.

2.3. Osteoblast/osteoclast co-culture

Bone marrow cells were isolated from the long bones of SAS Sprague Dawley wild type rats and differentiated into osteoclasts. Rats were anesthetized with isoflurane and euthanized in accordance with federal animal welfare guidelines and protocols reviewed and approved by the Lehigh Institutional Animal Care and Use Committee. Femurs were isolated and both ends of the bones were cut off. After transferring the bones to 1.5 ml conical tubes, they were centrifuged at 2000 rpm for 15 s to extract the marrow as essentially described by Dobson *et al* [19]. BMD cells were seeded onto either glass coverslips or TAMP scaffolds with the addition of MC3T3-E1 cells. Approximately 400 000 MC3T3-E1 cells were seeded together with BMD cells derived from one rat bone. The co-cultures were maintained in complete α-MEM as described above for osteoblasts with the addition of 50 ng ml^{-1} macrophage colony stimulating factor (MCSF) (Prospec, Israel, Cat. # cyt-046) to promote survival and differentiation of the osteoclast precursor cells [20]. In order to allow for better imaging of osteoclasts, most other cells from the co-culture were removed by incubation with Cellstripper® (Corning, Inc., Corning, NY, Cat. # 25-056-CI) using the following procedure. Medium was removed and each sample was washed with PBS. Cell stripper was added to the dish and incubated for 10 min at 37 °C. The Cellstripper® solution was pipetted aggressively over the sample to ensure the removal of unwanted cells. Samples were fixed for visualization by immunofluorescence detection as described below. As a control, osteoblasts/osteoclasts were co-cultured on coverslips and analyzed in parallel. The ratio of osteoblasts to osteoclasts was estimated by counting the number of nuclei not found in an osteoclast as determined by DAPI and Alexa488-phalloidin staining.

2.4. Scanning electron microscopy (SEM) analyses

Cells were fixed and dehydrated following standard EM sample preparation procedures including fixation in 4% glutaraldehyde at 4 °C overnight followed by gentle dehydration in a diluted ethanol series (2× 35%, 60%, 10 min each; 80%, 90%, 100% ethanol, 15 min each). Finally samples were incubated for 10 min in hexamethyldisilazane (Sigma, St. Louis, MI, cat. # 52619) for complete moisture removal [4]. Samples were stored in a desiccator until analyzed. Just before examination, samples were sputter coated with iridium using a turbo pumped sputter coater (Electron Microscopy Sciences—EMS575X) for 1 min to prevent charging. Samples were imaged with a Hitachi

4300 FEG SEM using secondary electron collection mode and 5.0 kV accelerating voltage. Cell spreading was analyzed in these images using the outline function of ImageJ software. 30–40 cells per time point were analyzed.

2.5. Proliferation of MC3T3-E1 cells on TAMP scaffolds

To quantitatively obtain accurate numbers of cells growing on TAMP scaffolds and avoid detection interference by bovine serum albumin (BSA), a cell culture medium-component that adsorbs extensively to TAMP scaffolds, a constitutively expressed large molecular weight protein, α-adaptin (MW, 112 kDa) was analyzed by Western blot using an α-adaptin-specific antibody (mouse monoclonal, BD Biosciences, San Jose, CA, Cat. # 610501). Briefly, MC3T3-E1 cells were seeded onto TAMP scaffolds as described above. At each time point, the TAMP scaffolds were crushed in 4× Laemmli sample buffer, boiled for 5 min, centrifuged to pellet the scaffold debris, and the supernatants were loaded onto a 10% SDS-PAGE gel. Gels were electrophoresed at 120 V for 90 min followed by transfer to nitrocellulose membranes for 90 min at 120 V on ice. After transfer, the membranes were blocked in 5% fat-free dry milk solution prepared in TBS with 1% Tween for 1 h at room temperature, rinsed briefly with TBS to remove excess blocking solution, and probed with primary antibody (1:2000 dilution in 5% BSA solution) overnight at 4 °C. The membranes were incubated with HRP conjugated goat-anti-mouse secondary antibody (1:5000, Life Technologies, Eugene, OR. Cat. # G21040) at room temperature for 1 h, and protein was detected using x-ray film and enhanced chemiluminescent reagent. Densitometry was performed using ImageJ software. The number of cells per TAMP scaffold ($n = 4$) was calculated by generating a standard curve of α-adaptin using a Western blot sample derived from 1 million cells.

2.6. Immunofluorescent staining of cells on TAMP scaffolds

Cells were processed for analysis by fluorescence detection of nuclei by incubating in DAPI (Molecular Probes, Eugen, OR, Cat. # D1306), actin using Alexa488- or Alexa568-phalloidin (Molecular Probes, Grand Island, NY, Cat. # A-12379), and specific antibodies by immuno-staining for vinculin (mouse monoclonal, Sigma, St. Louis, MO, Cat. # V9131), osteopontin (OPN) (rabbit polyclonal, AnaSpec, Fremont, CA, Cat. # 55455), osteocalcin (OCN) (rabbit polyclonal, Abbiotec, San Diego, CA Cat. # 250483), and TRAP (goat polyclonal, Santa Cruz, Dallas, TX Cat. # sc-30833). In brief, cells were fixed using 3.7% formaldehyde followed by permeabilization with 0.2% Triton X-100 for staining with the vinculin, OCN, and TRAP antibodies. Alternatively cells were fixed and permeabilized using ice-cold ethanol for OPN staining. Cells were then blocked in 5% BSA/PBS at room temperature overnight. The primary antibodies were diluted in blocking solution to 1:200 and incubated with cells at room temperature for 1 h. Blocking solution containing DAPI (1 μg ml^{-1}), Alexa488-phalloidin (1:100) and secondary antibody (1:200) (anti-vinculin, Alexa568-conjugated goat-anti-mouse, Molecular Probes/Invitrogen, Grand Island, NY, Cat. # A11031), Alexa568-phalloidin (1:100) and secondary antibody (1:200) (anti-TRAP, Alexa488-conjugated donkey-anti-goat, Molecular Probes/Invitrogen, Grand Island, NY, Cat. # A11055), and Alexa488-conjugated goat-anti-rabbit (Molecular Probes/Invitrogen, Grand Island, NY, Cat. # A11008) for OPN and OCN was incubated with the cells at room temperature for 1 h. Samples were imaged by submersing the scaffolds in PBS on a glass bottom 3.5 cm tissue culture dish (MatTek, Ashland, MA, Cat. # P35GCol-1.5-14-C) with the side on which cells were seeded facing the bottom. Imaging was performed using a Nikon Eclipse TE2000-E inverted fluorescence microscope equipped with 10× air, 20× air, 40× oil objectives and a forced-air cooled Photometrics CoolSnap HQ CCD camera (Roper Scientific, Martinsried, Germany). Images were captured using MetaVue (Molecular Devices, Sunnyvale, CA) software version 6.1r5. Average surface area per cell was quantitated for 30–40 cells/time point using the outline function of the ImageJ software package.

2.7. qRT-PCR analyses of cells grown on TAMP scaffolds

MC3T3-E1 cells were seeded onto TAMP scaffolds and grown for 1, 7, 16 or 32 d before collection of RNA using either Arcturus® Picopure RNA isolation kits (Applied Biosystems, Carlsbad, CA Cat # Kit0204) or Qiagen RNeasy mini kits (Qiagen, Valencia, CA, Cat. # 74104). cDNA was synthesized from these samples using SuperScript III First-strand synthesis (ThermoFisher, Carlsbad, CA, Cat # 18080-051). Analysis of samples was performed using either Osteogenesis PCR arrays (SA Biosciences, Frederick, MD, Cat # PAMM-026Z) and RT^2 Real-time SYBR green PCR master mix (SA Biosciences, Frederick, MD, PA-012-12) on a model 7300 Thermocycler (Applied Biosystems), or SYBRgreen-Rotorgene PCR kit (Qiagen, Valencia, CA, Cat. # 204074) and sets of custom-designed oligonucleotides (Integrated DNA Technologies, Coralville, IA) that corresponded to the mRNAs encoding the relevant proteins on a Rotor-gene real-time PCR cycler. GAPDH was analyzed in parallel and used as expression reference. Fluorescence signal detection within 35 PCR cycles was considered significant. mRNA level fold-change was normalized against GAPDH expression and compared to day 0.

2.8. Alkaline phosphatase (ALP) activity assay

MC3T3-E1 cells were grown on TAMP scaffolds, and samples were collected for ALP activity analysis on days 3, 7, 11, 14 and 21. Samples were prepared by washing in TBS followed by incubation in 500 μl lysis buffer (TBS, 0.5% SDS, and protease inhibitor cocktail (1:100), Sigma, Cat. # P8340) with agitation for 15 min on ice. 20 μl of cell lysate was mixed with 20 μl of 2× sample buffer and boiled for determination of cell number as described above. ALP activity was measured quantitatively using a colorimetric Quantichrom ALP detection kit (BioAssay Systems, Hayward, CA, Cat. # DALP-250). Briefly, 50 μl of cell lysate was incubated with 150 μl of ALP buffer (containing 10 mM p-nitrophenol phosphate and 5 mM MgAcetate) per reaction at room temperature for 1 h. The activity of ALP was determined by measuring the absorbance at 405 nm using a Tecan Infinite M200 PRO plate reader spectrophotometer. ALP activity was normalized to cell number as determined by Western blot detection of α-adaptin ($n = 4$).

2.9. TRAP staining of osteoclasts grown on TAMP scaffolds

A co-culture of MC3T3-E1 and BMD cells were grown on TAMP scaffolds in parallel to TAMP scaffolds seeded with MC3T3-E1 cells only for 10 d as described above. Next, the samples were fixed in 3.7% formaldehyde, stained with DAPI and imaged. The same samples were then stained for TRAP activity using an Acid Phosphatase, Leukocyte (TRAP) Kit (Sigma, St. Loius, MO, Cat. # 387A-1KT). In brief, scaffolds were incubated for 1 h in staining solution, which contained tartrate to render all other phosphatases inactive, and the substrate Naphthol AS-BI that couples with fast garnet GBC on enzymatic hydrolysis to form a red insoluble product. The samples were washed 3 times in dH_2O following staining and imaged at 4× using a Nikon SMZ1500 dissection scope equipped with an HR plan Apo 1× WD 54 Nikon objective and a Nikon DS-Fi2 digital camera operated by NIS Elements F4 32 bit software. The stain was quantified using ImageJ software by analyzing the amount of red in each image (5 images per condition ($n = 3$ independent experiments)) and normalized by subtracting background obtained on TAMP scaffolds stained without cells.

2.10. Statistical analyses

Unpaired student t-tests were used to analyze statistical significance. Data are presented as mean ±SEM with a p-value < 0.05 to be considered significant.

3. Results

3.1. TAMP scaffold composition and porosity

To perform a careful analysis of the biological performance of TAMP material using advanced *in vitro* proliferation and differentiation assays, we produced circular, dual-porous disc shaped TAMP scaffolds of 70 mol% SiO_2 and 30 mol% CaO model composition with a diameter of approximately 13 mm and a height of approximately 2 mm, using a modified sol-gel fabrication procedure (figure 1(a)) [4, 5]. TAMP scaffolds featured interconnected macro-pores ranging from 20 to 200 μm measured by mercury porosimetry and as seen in SEM micrograph in figure 1(b), and interconnected nano-pores ranging from 2.5 to 50 nm measured by BET nitrogen adsorption and imaged by SEM (see figure 1(c)). BET analyses, revealed a surface area of 90.2 ± 5.5 $m^2\,g^{-1}$ (figure 1(d)). Additionally, when incubated in simulated body fluid (SBF) or cell culture medium, TAMP scaffolds become coated with a crystalline layer of hydroxyapatite, which contributes to the glass' biocompatibility (figure 1(e)) [4, 5]. Further, TAMP scaffolds dissolved with a half-life dissolution of 15.4 d under quasi-dynamic conditions [8]. Taken together these characteristics suggest that TAMP scaffolds fulfill many parameters desirable of an advanced bioactive material for hard tissue regeneration.

3.2. Pre-osteoblast cells adhere to the surface of TAMP scaffolds

TAMP scaffold opaqueness due to porosity (figure 1(a)) interferes with detection of cells growing on the scaffold surface by standard transmission light microscopy. Therefore, SEM was used for observing the cells on scaffolds directly (figure 2(a)-previously published in [21] as illustration of method). In addition, to determine whether cells were forming stable adhesions when growing on the scaffolds, they were fluorescently stained for actin (Alexa488-labeled phalloidin, green), chromatin (cell nuclei, DAPI, blue), and vinculin (using anti-vinculin specific and Alexa568-labeled secondary antibodies, red), a protein component of focal adhesion complexes responsible for forming cellular adhesions to substrates (figure 2(b)). One hour post seeding onto the scaffolds, MC3T3-E1 pre-osteoblast cells remained largely rounded, although they had attached to the scaffold surface as indicated by the formation of numerous filopodial anchoring extensions (figure 2(a), 1 h, depicted with white arrows). Additionally, actin remained diffuse and located cortically as indicated by the bright staining at the cell periphery, which is typical for not yet well-attached cells stained shortly after seeding (figure 2(b), top panel). Vinculin was detectable after 1 h mainly as a soluble cytoplasmic pool, which is typical for vinculin that is not bound to focal adhesions [22]. After 2 (figures 2(a), (b), second row) and especially after 8 h post seeding (figures 2(a), (b), third row), cells were spreading to acquire their typical flat morphology. In addition, cells had formed numerous lamellipodial extensions. Actin began to form distinct stress fibers as indicated by the filamentous staining pattern (figure 2(b), third row, depicted with

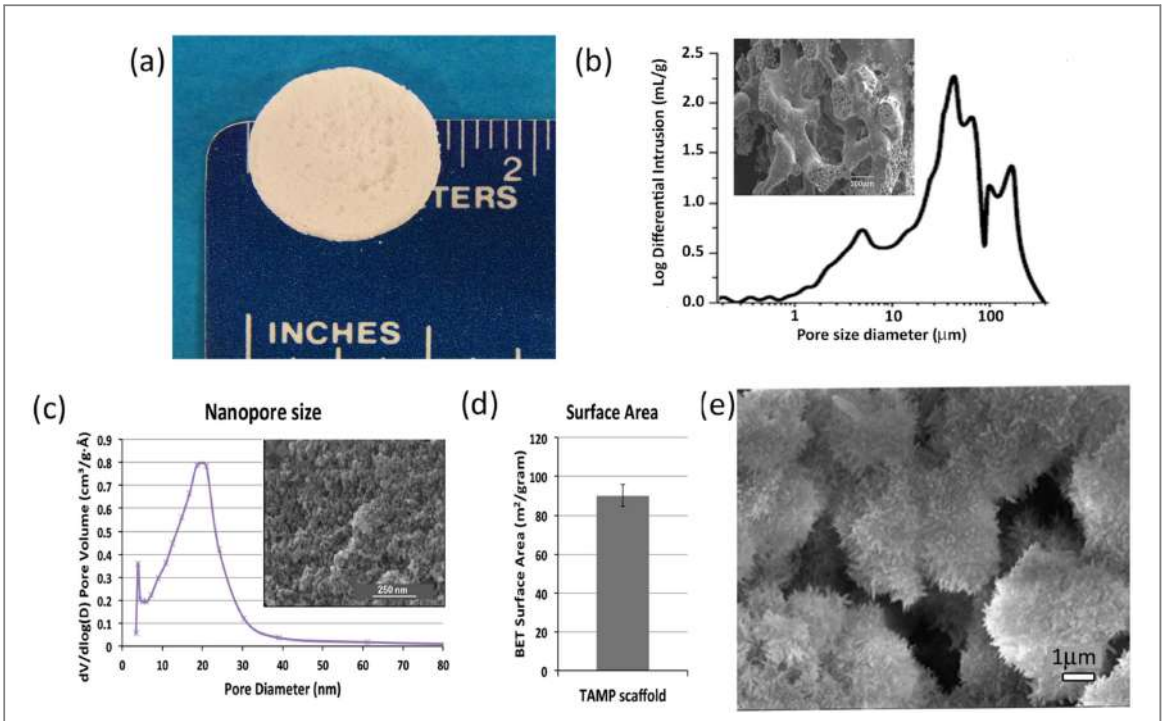

Figure 1. TAMP scaffold porosity and hydroxyapatite formation in physiological solutions. (a) TAMP scaffolds implemented in the analyses described here were manufactured as opaque discs of approximately 13 mm diameter and 2 mm thickness. (b) SEM analyses revealed the highly porous structure of the TAMP scaffolds including interconnected macro and (c) nanopores. Mercury porosimetry and BET nitrogen adsorption analyses revealed a pore size ranging from approximately 20 to 200 μm for macropores and 2.5–50 nm for nanopores, respectively. (d) BET analyses further revealed a TAMP surface area of 90.2 $\pm$ 5.5 m^2 g^{-1}. (e) SEM analyses additionally revealed that TAMP scaffolds develop a robust layer of hydroxyapatite (HA) on their surface when incubated for 3 d in physiological solutions, such as SBF (shown here) or PBS (Kowal *et al*, unpublished). (e) Adapted from [5] with permission from John Wiley and Sons.

yellow arrows). After 3 d, a dense layer of cells, partially growing on top of each other featuring numerous filopodial and lamellipodial extensions were observed by SEM (figure 2(a), bottom row). Pronounced focal adhesion complexes formed at the tip of robust actin stress fibers (figure 2(b), bottom row, depicted with orange arrows) as is typical of cells growing on stiff substrates [23–25], indicated that cells had established healthy attachments to the surface of the TAMP scaffold material. Consistent with these data, cells could not easily be removed from TAMP scaffolds even after extended exposure to trypsin (a protease commonly used to release MC3T3-E1 and other cell types from tissue culture plates), suggesting that cells attached robustly to TAMP scaffolds. Average surface area per cell was quantitated for 30–40 cells/time point using the outline function of the ImageJ software package (figure 2(c)), further supporting that cells were spreading over time. Note the relatively large standard deviations are due to the 3D nature of the TAMP scaffolds, which allows cells to grow in many different directions relative to the image plane.

3.3. MC3T3-E1 cells colonize the inside of TAMP scaffolds

As analyses by SEM showed that [1] cells covered the majority of the scaffold surface after 8 h (figure 3(a), top panel), [2] cells continued to proliferate to form a dense monolayer on the TAMP scaffold surface (supplemental figure 1 is available online at stacks.iop.org/BMM/13/025005/mmedia, days 10 and 21), and [3] cells were growing at the entrance of macro-pores (figure 3(a)), we investigated whether MC3T3-E1 cells would also colonize the TAMP scaffold interior. Cells were seeded onto the TAMP scaffolds and fixed 10 d post seeding, then a center section was cut out, turned on its side and mounted. SEM analyses of these cross-sections showed cells growing inside the TAMP scaffolds, indicating that cells had migrated into the macro-pores and were also colonizing the inside of the TAMP scaffolds (figure 3(b)). These results were validated by a complementary experiment in which cross-sections from days 1, 3, and 10 post cell seeding were stained by DAPI to visualize cell nuclei. The images show that initially (figure 3(c)—day 1), cells attach to the surface and inside of surface exposed macro-pores. Over time however, the cells infiltrated deep into the macro-pores and can be seen in the inner matrix of the TAMP scaffolds. This is particularly evident in the day 10 image (figure 3(c)—2 left most yellow arrows. Note that not all cells are visible due to uneven surface topology of the sections.

To accurately determine the duplication rate of cells proliferating on TAMP scaffolds, we established a technique that allowed us to accurately assess the number of cells on and inside the scaffolds at

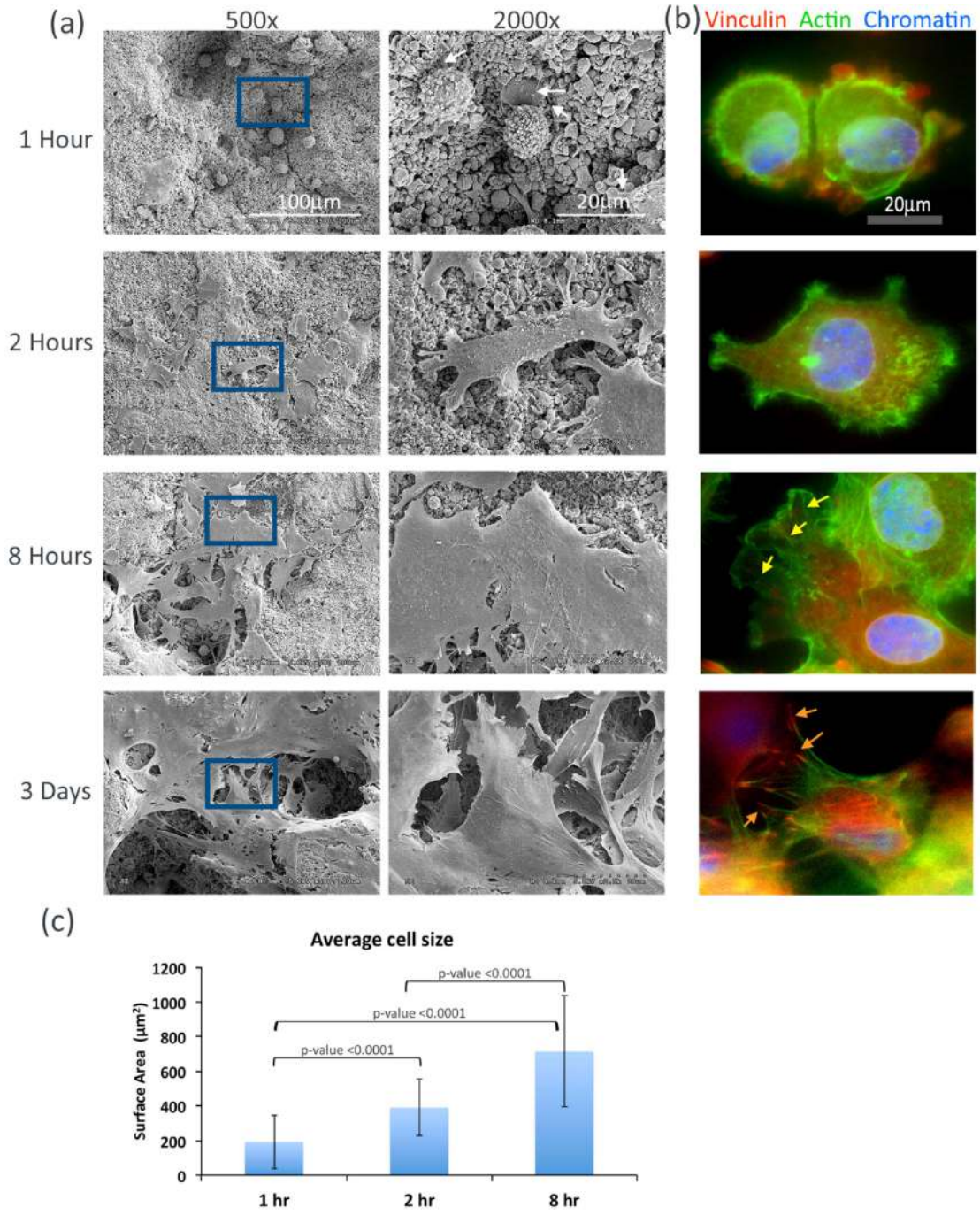

Figure 2. MC3T3-E1 pre-osteoblasts adhere to and colonize the surface of TAMP scaffolds. (a) MC3T3-E1 pre-osteoblast cells were seeded onto TAMP scaffolds, fixed and analyzed by SEM at indicated times. Note initial attachment of still rounded cells 1 h post seeding as indicated by filopodial extensions (depicted with arrows), successive cell spreading (2 h) and scaffold colonization by 8 h and 3 d. Boxed areas in A are shown at higher magnification on the right. (b) Fluorescence light microscopic analyses performed at the same time points by staining cells for actin (Alexa-488-phalloidin, green), vinculin (primary and Alexa568-conjugated secondary antibodies, red), and cell nuclei (DAPI, chromatin, blue) in addition revealed the formation of actin-based stress fibers (yellow arrows) and the formation of robust cellular focal adhesions (orange arrows) indicative of cell attachment occurring over time. Note that cells located in pores, as a result of depth perception, may appear smaller compared to cells growing on exposed surface areas (compare e.g. 1 h SEM and fluorescent images). (c) Average cell surface area at 1, 2, and 8 h post seeding quantified for 40–50 cells/time point using the outline function of the Image J software package. (a) Adapted from [21] with permission from the Royal Society of Chemistry.

progressive time points. Common techniques such as imaging would not capture cells growing inside the scaffolds. In addition, proteins such as BSA, MW: 66 kDa, an abundant serum component of cell culture medium, robustly absorbed to TAMP scaffolds (supplemental figure 2, marked with arrow) and interfered with standard quantitative colorimetric protein assays such as Bradford and MTS. We thus detected and quantified the levels of a constitutively expressed housekeeping protein, α-adaptin (a component of the endocytic adaptor protein 2 (AP-2) complex [26] by Western blot using α-adaptin specific antibodies

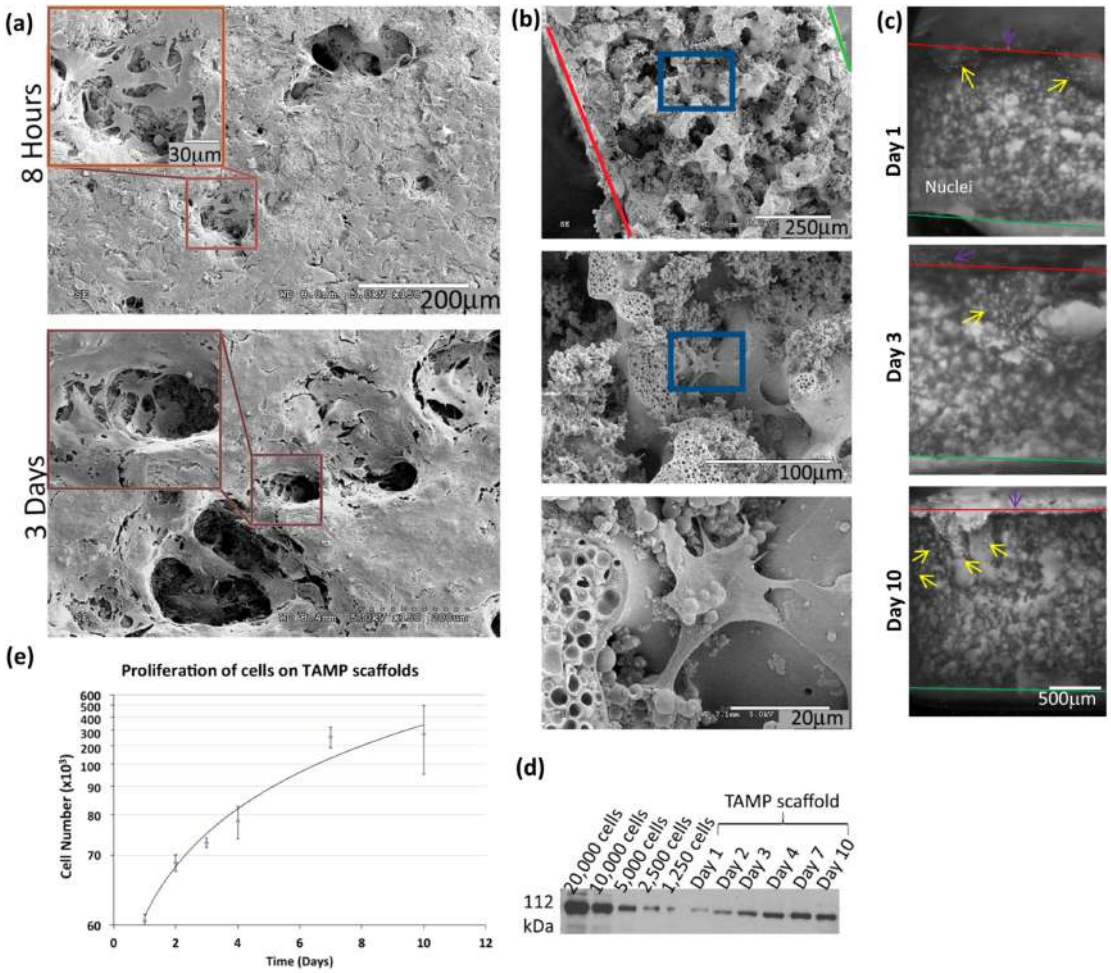

Figure 3. MC3T3-E1 cells proliferate on and inside TAMP scaffolds. (a) At seeded density, cells within 8 h spread over the surface of the TAMP scaffolds (top panel) and formed a dense monolayer within 3 d on its surface and at the entrance of macropores (bottom panel, boxed and enlarged areas) indicating that cells were also colonizing the inside of TAMP scaffolds. (b) To investigate this, scaffolds seeded with cells for 10 d were cut, turned sideways and imaged by SEM (red line indicates top of scaffold onto which cells were seeded, green line indicates bottom side of TAMP scaffolds; boxed areas are shown magnified below). (c) Cells stained with DAPI (cell nuclei) detected on fluorescence images inside the scaffolds 3 and 10 d after seeding (delineated with yellow arrows) demonstrate that MC3T3-E1 cells infiltrate into macropores to colonize the interior of the scaffold matrix. Purple arrows indicate cells on the TAMP surface. (d) To accurately quantify cell numbers on TAMP scaffolds, α-adaptin, a MC3T3-E1 cell endogenous housekeeping protein was quantified by Western blot analyses using α-adaptin-specific antibodies. (e) Cell quantitation at indicated time points revealed that MC3T3-E1 cells proliferating on TAMP scaffolds entered the logarithmic growth phase of proliferation by approximately day 2 and growth plateaued at approximately day 10, resulting in a deduced duplication time of app. 3 d under standard cell culture conditions.

(figure 3(d)). While the detection of smaller standardly used house-keeping proteins such as actin, tubulin and GAPDH which migrate faster on SDS-PAGE gels than BSA was impeded (supplemental figure 2), the large molecular weight of α-adaptin (MW: 112 kDa) allowed its accurate quantification. Based on these analyses, we found that MC3T3-E1 cells proliferating on TAMP scaffolds entered the logarithmic growth phase of proliferation by approximately day 2 and growth began to plateau at approximately day 10 (figure 3(e)). Logarithmic growth resulted in a duplication time of app. 3 d under standard cell culture conditions, slower than proliferation on tissue culture plastic (app. 38 h according to ATCC), suggesting that cells may have begun to differentiate.

3.4. MC3T3-E1 cells differentiate into mature osteoblasts when grown on TAMP scaffolds: quantitative transcription analyses

To assess whether MC3T3-E1 pre-osteoblasts differentiate into mature osteoblasts when grown for extended periods on TAMP scaffolds, we quantitatively analyzed transcription of osteoblast differentiation-related genes (including genes related to [1] cell adhesion [labeled orange in figure 4(a)], [2] extracellular matrix and remodeling [light blue], [3] proliferation [olive], [4] differentiation [gray], [5] collagen expression [off red], [6] bone specific transcription regulation [yellow] and [7] expression of osteoblast calcified matrix-specific proteins [purple]) by quantitative PCR analyses (qRT-PCR) using a commercially

(a)

Symbol	Gene Name	Array Loc.	Day 1	Day 7	Day 14	Day 26
Dmp1	dentin matrix acidic phosphoprotein 1	C10	67.1	24.4	23.9	10.8
Itgam	integrin, alpha M	E3	350.4	20.7	20.5	8.8
Ahsg	alpha-2-HS-glycoprotein	A1	66.8	24.4	3.0	3.0
OCN	osteocalcin	N/A	-	5.3	18.7	45.3
Col4a2	collagen, type IV, alpha 2	C1	24.9	3.8	4.2	4.6
Itga3	integrin, alpha 3	E2	7.7	3.3	2.8	1.3
Nfkb1	nuclear fact. of κ light polypep. gene enhanc. in B-cells 1	E11	7.2	4.3	3.4	1.5
Tgfb1	transforming growth factor, beta 1	F12	6.5	2.7	5.2	5.5
Vegfa	vascular endothelial growth factor a	G11	16.5	4.3	3.6	1.9
Col4a1	collagen, type IV, alpha 1	B12	3.2	4.3	4.1	6.6
Phex	phosphate regulating endopeptidase homolog, X-linked	F1	4.4	-1.1	7.3	2.0
OPN	Osteopontin	N/A	-	3.5	1.8	6.5
Mmp9	matrix metallopeptidase 9	E9	6.4	1.3	1.5	2.0
Col1a1	collagen, type I, alpha 1	B8	3.1	3.9	3.2	5.4
Fgf2	fibroblast growth factor 2	D2	2.5	4.8	3.8	1.7
Col5a1	collagen, type V, alpha 1	C2	3.1	2.7	2.1	5.1
Fn1	fibronectin 1	D7	4.0	2.6	2.4	3.5
Ctsk	cathespsin K	C9	3.1	1.6	2.8	2.9
Scarb1	scavenger receptor class B, member 1	F3	1.9	2.1	1.5	1.5
Tgfb3	transforming growth factor, beta 3	G2	2.4	1.3	4.2	2.9
Anxa5	annexin A5	A4	1.8	2.2	1.4	1.6
Col6a2	collagen, type VII, alpha 2	C4	2.4	1.8	-1.1	1.7
Bmp4	bone morphogenetic protein 4	A9	2.6	1.5	-1.2	1.6
Bgn	biglycan	A5	1.2	2.6	2.2	2.8
Pdgfa	platelet-derived growth factor alpha polypeptide	E12	-1.0	2.7	2.3	2.4
Itgb1	integrin, beta 1	E5	2.1	2.2	1.4	1.4
Itgav	integrin, alpha V, vitronectin receptor	E4	1.7	1.5	1.1	1.4
Cd36	CD36 molecule, thrombospondin receptor	B2	1.4	2.3	1.3	1.8
Serpinh1	serpin peptidase inhibitor, clade H, member 1	F4	1.1	1.7	1.2	1.8
Cdh11	cadherin 11, type 2, OB-cadherin	B3	1.2	1.6	-1.2	1.2
Bmpr1b	bone morphogenetic protein receptor, type IB	B1	152.2	188.0	-	-
Itga2	integrin, alpha 2	D12	-	35.5	20.0	-
Col7a1	collagen, type VII, alpha 1	C5	-	49.5	-	5.2
Icam1	intercellular adhesion molecule 1	D9	-	62.8	-	6.3
Fgf1	fibroblast growth factor 1	D1	-	-	12.4	-
Ambn	ameloblastin, enamel matrix protein	A3	-	-	-	3.5
Bmp3	bone morphogenetic protein 3	A8	-	-	-	1.5
Tuft1	tuftelin 1	G7	-	-	-	4.5
Bmp6	bone morphogenetic protein 6	A11	12.0	2.4	4.0	-4.4
Tgfbr2	transforming growth factor, beta receptor 2	G4	-1.6	3.9	2.5	2.0
Flt1	fms-related tyrosinase kinase 1	D6	2.1	3.1	-1.0	-1.5
Sox9	SRY box 9	F10	4.4	1.9	-1.3	-1.8
Itga2b	integrin, alpha 2b	E1	6.5	2.1	1.2	-2.0
Alpl	alkaline phosphatase, liver/bone/kidney	A2	5.2	1.0	-4.3	2.8
Tfip11	tuftelin interacting protein 11	F11	-2.2	2.5	1.5	-1.3
Col12a1	collagen, type XII, alpha 1	B6	-1.3	3.2	1.1	1.6
Bmp 1	bone morphogenetic protein 1	A6	2.8	1.2	1.3	-1.6
Comp	cartilate oligomeric matrix protein	C6	3.5	-1.4	-6.4	-1.3
Smad3	SMAD family member 3	F7	1.3	1.8	1.3	-1.6
Vegfb	vascular endothelial growth factor b	G12	-1.5	1.4	1.7	1.3
Runx2	runt-related transcription factor 2	F2	-2.0	2.4	1.0	-1.1
Fgfr1	fibroblast growth factor receptor 1	D4	1.7	1.3	-4.2	-2.3
Col2a1	collagen, type II, alpha 1	B10	5.8	-2.4	1.6	-2.4
Smad2	SMAD family member 2	F6	3.0	-2.0	-1.1	-1.8
Col11a1	collagen, type XI, alpha 1	B5	-1.8	-1.7	-1.3	2.3
Egf	epidermal growth factor	C11	3.2	-1.6	-7.0	-2.2
Col10a1	collagen, type X, alpha 1	B4	-2.6	-2.2	-1.5	2.9
Msx1	msh homeobox 1	E10	1.2	1.3	-2.0	-1.5
Igf1r	insulin-like growth factor 1 receptor	D11	-1.4	1.4	-1.6	-1.1
Twist1	twist homolog 1	G8	-1.4	1.3	-2.0	-1.4
Tgfbr3	transforming growth factor, beta receptor 3	G5	-1.2	-5.7	1.1	1.3
Smad4	SMAD family member 4	F8	-1.0	1.2	-1.4	-1.1
Col6a1	collagen, type VI, alpha 1	C3	1.0	1.1	-1.7	-1.1
Bmpr1a	bone morphogenetic protein receptor, type IA	A12	-2.8	-1.4	-2.1	-1.5
Igf1	insulin-like growth factor 1	D10	-8.3	-1.0	-3.9	-1.3
Tgfb2	transforming growth factor, beta 2	G1	-2.1	-3.1	-1.1	-1.4
Smad1	SMAD family member 1	F5	-1.3	-3.1	-1.5	-2.1
Vdr	vitamin D receptor	G10	-1.3	-2.4	-4.1	-4.6
Vcam1	vascular cell adhesion molecule 1	G9	-1.5	1.3	-1.9	-1.8
Col3a1	collagen, type III, alpha 1	B11	-1.9	-1.6	-2.4	-1.3
Col1a2	collagen, type I, alpha 2	B9	-2.1	-1.5	-2.3	1.1
Mmp2	matrix metallopeptidase 2	E7	-1.5	-2.4	-2.1	-1.4
Fgfr2	fibroblast growth factor receptor 2	D5	-9.6	-3.3	-3.3	-4.5
Csf2	colony simulating factor 2	C7	-	-	-	-
Enam	enamelin	C12	-	-	-	-
Fgf3	fibroblast growth factor 3	D3	-	-	-	-
Gdf10	growth differentiation factor 10	D8	-	-	-	-
Mmp10	matrix metallopeptidase 10	E6	-	-	-	-
Mmp8	matrix metallopeptidase 8	E8	-	-	-	-
Sost	sclerostin	F9	-	-	-	-
Tgfbr1	transforming growth factor, beta receptor 1	G3	-	-	-	-
Tnf	tumor necrosis factor	G6	-	-	-	-

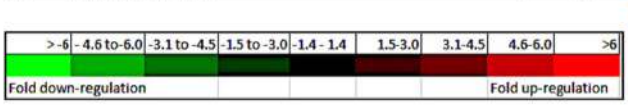

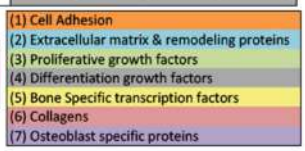

Figure 4. MC3T3-E1 cells differentiate into mature osteoblasts when grown on TAMP scaffolds. To investigate whether MC3T3-E1 osteoblast precursor cells differentiate into mature osteoblasts when grown on TAMP scaffolds we quantitatively determined expression of marker proteins at indicated times post seeding using (a) a bone-cell differentiation array (SA Biosciences/Qiagen) and quantitative reverse transcription polymerase chain reaction (qRT-PCR) analyses. Two missing, late osteoblast-specific marker proteins, osteocalcin (OCN) and osteopontin (OPN) were analyzed in addition using representative primer sets. Up-regulation (red), down-regulation (green), or unchanged (gray) mRNA expression levels for each analyzed protein are shown in the heat-map to the right. Representative proteins were grouped into categories including (1) cell adhesion proteins (orange), (2) extracellular matrix (ECM) and remodeling proteins (light blue), (3) proliferative growth factors (olive), (4) differentiation growth factors (gray), (5) bone-specific transcription factors (yellow), (6) collagens (off red), and (7) osteoblast specific proteins (purple). (b) Expression profiles of proteins of these categories were analyzed by trend lines. Note, that early gene up-regulation was found for genes related to categories (1)–(3), followed by expression of differentiation growth factors (category 4). Expression of the well-known bone cell differentiation transcription factor, Sox9, was high early, and was down regulated as RunX2 became up regulated (category 5). Finally, extracellular matrix components of bone, primarily collagens (category 6) and osteoblast specific extracellular matrix protein genes (category 7) were found to be expressed at late time points, collectively indicating osteoblast cell differentiation.

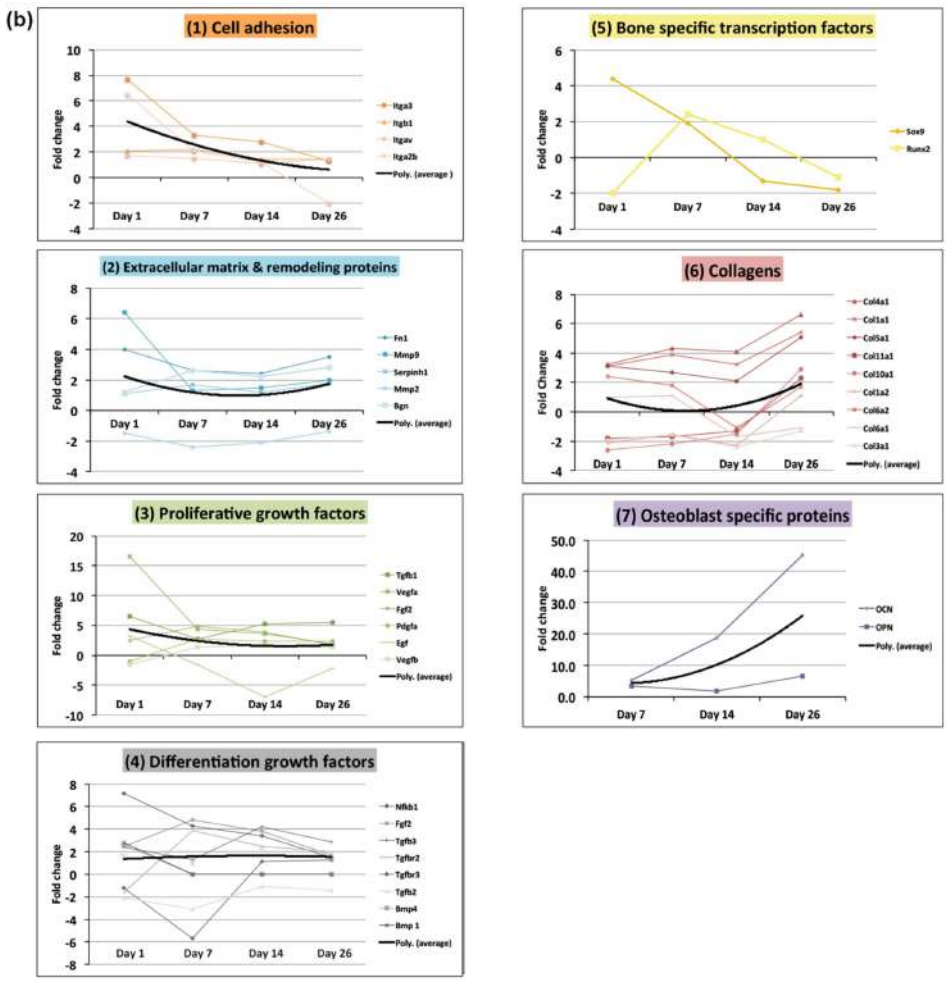

Figure 4. (Continued.)

available 84-gene bone differentiation array (SA-Biosciences) supplemented by a few additional well-known bone cell marker proteins (OCN, OPN) (figure 4(a)). Genes that were not evaluated because they showed unrealistically high up-regulation profiles, did not obviously fall into one of the above described categories, their relation to bone-cell differentiation remains unclear, or their expression pattern remained unchanged, are shown in white.

RNA was isolated, quantified, and normalized on days 1, 7, 14, and 26 post seeding. We found that representative genes were either up (figure 4(a), labeled red) or down regulated (figure 4(a), labeled green), or that their expression levels remained unchanged (figure 4(a), gray). Gene expression profiles of differentiating pre-osteoblasts have been well characterized [27–29], and the overall trends in gene expression observed here for MC3T3-E1 cells growing on TAMP scaffolds are consistent with pre-osteoblast cells attaching to their substrate, proliferating, and differentiating into mature, calcified matrix secreting osteoblasts. For example, the overall trend in gene expression for cell adhesion proteins (figure 4(b), panel 1; black polynomial average line in all graphs indicates functional group trend) such as those encoding integrins α3, β1, αv, α2b (respective gene names: Itga3, Itgb1, Itgav, and Itga2b) was initially high and was down-regulated over time indicating that cells were expressing genes relevant for making initial attachments to the TAMP scaffold surface. Additionally, secreted extracellular matrix and matrix-remodeling proteins such as fibronectin (Fn1), biglycan (Bgn), Serpin h1 peptidase inhibitor (Serpinh1), and matrix metalloproteases (Mmp2, Mmp9) (figure 4(b), panel 2) were up regulated early (at day 1). Further, several growth factors related to proliferation (such as Tgfb1, Vegfa, Fgf2, Pdgfa, Egf, Vegfb) were more highly expressed on day 1 and were down-regulated over time (figure 4(b), panel 3), whereas other growth factors related to differentiation of MC3T3-E1 cells (such as Nfkb1, Fgf2, Tgfb3, Tgfbr2, Tgfbr3, Tfgb2, BMP1, BMP4) (figure 4(b), panel 4) were expressed consistently, suggesting that throughout the time course, cells continuously expressed growth factors relevant to differentiation. The two main transcription factors for bone cell differentiation were both up-regulated early, with Sox9 elevated at day 1 and Runx2 elevated at day 7 (figure 4(b), panel 5), while collagens

(Col1a1, Col1a2, Col3a1, Col4a1, Col5a1, Col6a1, Col6a2, Col10a1, Col11a1) were upregulated both early and late (figure 4(b), panel 6). ALP mRNA levels, an enzyme that is up regulated in pre-osteoblasts during their differentiation into mature osteoblasts, was up-regulated early (figure 4(a)). OCN and OPN, both late indicators of bone cell differentiation, were up regulated at later time points (figure 4(b), panel 7). Taken together, these quantitative RNA analyses indicate that MC3T3-E1 cells express genes relevant for adhesion, proliferation, and differentiation into mature osteoblasts when grown for 4 weeks on TAMP scaffolds.

3.5. MC3T3-E1 cells differentiate into mature osteoblasts when grown on TAMP scaffolds: bone cell marker protein expression

ALP enzyme expression and activity are canonical indicators of osteoblast differentiation and are known to be up-regulated during osteoblast differentiation [30, 31]. Increased expression of the ALP gene in MC3T3-E1 cells growing on TAMP scaffolds was observed as described above (figure 4(a)). Consistent with these data, colorimetrically assessed enzymatic ALP activity increased almost three-fold from days 3 to 21 (figure 5(a)). These data are also in agreement with the decreased proliferation rate of MC3T3-E1 cells grown for 3–4 weeks on TAMP scaffolds (figure 3(c)) as cell proliferation and differentiation are known to be cross-correlated [32].

Mature osteoblasts are also known to express and secrete proteins that aid in the formation of secreted calcified bone-specific extracellular matrix, such as OCN and OPN. To verify that the observed up-regulation of mRNA expression for OCN and OPN was also detectable as an up-regulation in protein expression, we used specific antibodies and immunofluorescence microscopic analyses to examine OCN and OPN protein expression of MC3T3-E1 cells growing on TAMP scaffolds over time (figures 5(b), (C)). OCN staining on day 3 presented as a diffuse perinuclear staining, whereas staining on day 10 resulted in both, diffuse perinuclear staining and some defined puncta localized in the cytoplasm and/or extracellular matrix, which increased in number and size by days 16 and 32, while diffuse cellular staining diminished (figure 5(b), labeled with arrows). Since OCN is a late differentiation marker, its expression/staining pattern is consistent with the expected and previously observed late mRNA up-regulation of this secreted protein. OPN is another late up-regulated, bone-specific matrix protein. Consistently, only diffuse OPN staining was observed on days 3, 10 and 16 (figure 5(c)), that either indicates early cytoplasmic expression similar to the expression profile observed for OPN, or unspecific background staining (see supplemental figure 3). In contrast, a prominent punctate OPN stain comparable to the late OCN stain was detected on day 32 (figure 5(c), labeled with arrows), suggesting a robust OPN expression of MC3T3-E1 cells growing on TAMP scaffolds at later time points. Taken together, these quantitative and qualitative marker protein expression analyses reiterate that MC3T3-E1 cells appear to differentiate into mature osteoblasts when growing on TAMP scaffolds.

3.6. TAMP scaffolds promote the growth of co-cultured osteoblasts and osteoclasts into actively remodeling bone tissue-like arrangements

Since bone is a highly dynamic organ that is constantly remodeled by synthesis and degradation (via osteoblasts and osteoclasts, respectively) [33], we wanted to test whether TAMP scaffolds also support the growth of osteoclasts and whether co-culture of osteoblasts and osteoclasts would remodel TAMP scaffolds similarly to natural bone. Osteoclasts feature a number of morphological characteristics including a very large cell size, multiple cell nuclei, relatively large vesicular inclusions, and a sealing zone composed of actin and vinculin. Because osteoclasts mature via the fusion of several precursor cells and thus contain multiple cell nuclei, they no longer proliferate making it necessary to differentiate these cells from their precursors located in bone marrow. BMD cells and MC3T3-E1 cells were grown as co-cultures with culture medium supplemented with MCSF to promote the survival and differentiation of the osteoclast precursor cells (reviewed in [34–36]). Maturing MC3T3-E1 cells are known to enhance osteoclastogenesis [37, 38] through secretion of receptor activator of nuclear factor kappa-B ligand, the main cytokine that regulates osteoclast differentiation and activation [34–36]. After 10 d of co-culture on microscopic cover slips, mature osteoclasts were clearly recognizable based on the above described morphological features on both differential interference contrast (DIC) as well as fluorescent images (after staining nuclear chromatin and actin) (figure 6(a)). Remarkably, co-culturing these cells for 10 d on TAMP scaffolds resulted in the formation of a complex tissue structure that consisted of a dense network of MC3T3-E1 osteoblasts (recognizable by their small size), and interspersed osteoclasts (recognizable by their large size, multiple cell nuclei, and their typical actin-based sealing zones) (figure 6(B), labeled with OC and outlined with dashed lines). Single channel black and white images of actin (figure 6(b), top) and DAPI (cell nuclei, figure 6(b), bottom) further supported these distinctive osteoclast features (depicted with arrows). Quantitative analyses revealed a ratio of 179 $\pm$ 53 osteoblasts per osteoclast, a ratio similar to the ratio of these two cell types in human (iliac crest bone; [39] (figure 6(c)).

To further support our conclusion that the large multi-nucleated cells indeed represented osteoclasts, we treated co-cultured TAMP scaffolds with Cellstripper® (Corning), a proprietary mixture of

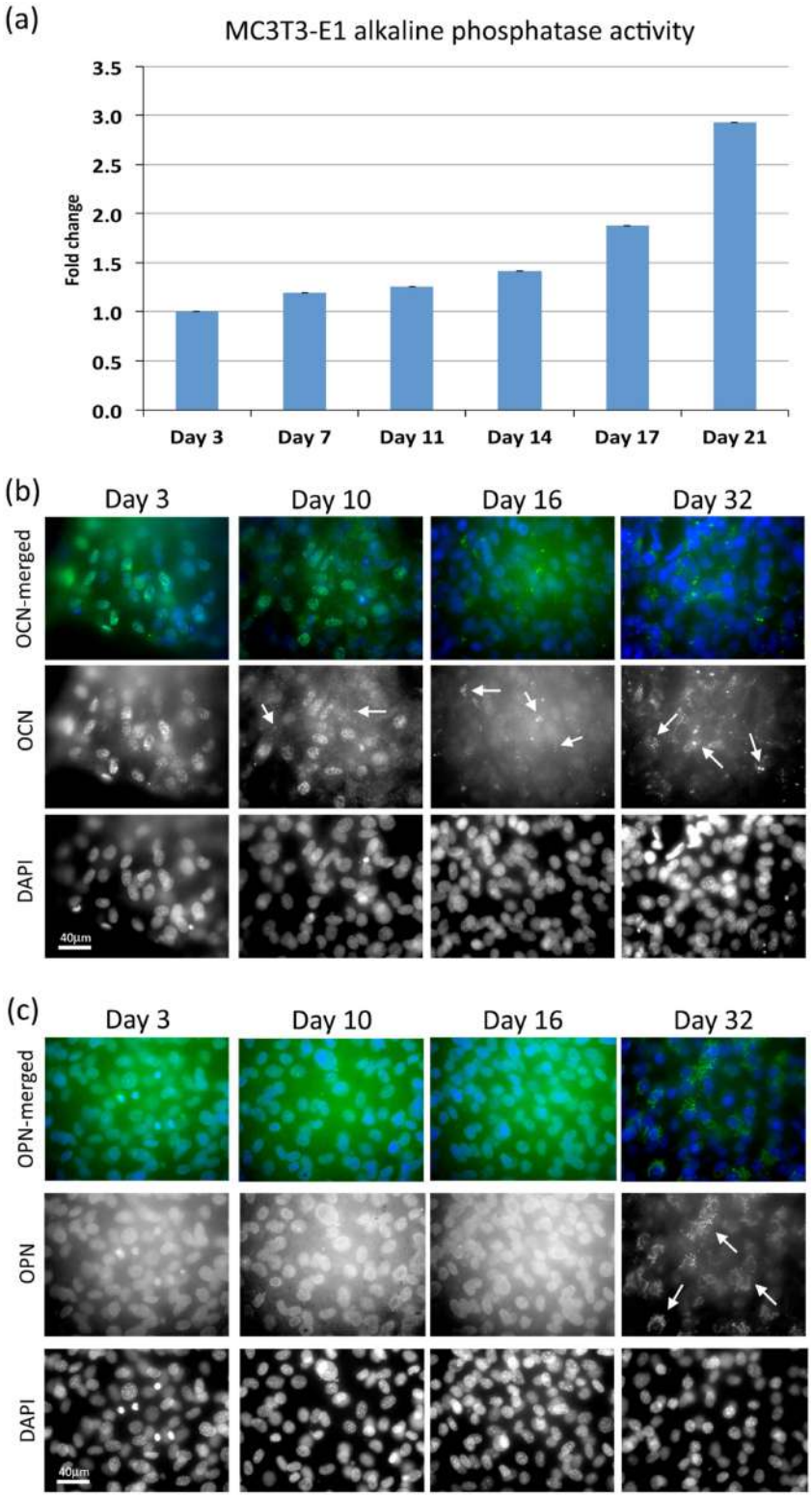

Figure 5. MC3T3-E1 cells produce and secrete bone-specific proteins when grown on TAMP scaffolds. (a) MC3T3-E1 cells were grown on TAMP scaffolds, and alkaline phosphatase (ALP) enzyme activity was analyzed colorimetrically at indicated days post cell seeding. Note, continually increased ALP activity that increases almost exponentially at later time points (days 17, 21), which correlates with reduced cell proliferation and increased differentiation. Similarly, MC3T3-E1 cells were grown on TAMP scaffolds for indicated times, and analyzed for (b) osteocalcin (OCN), and (c) osteopontin (OPN) protein production/secretion using immunofluorescence microscopy with OCN and OPN-specific antibodies (green). Cell nuclei were stained with DAPI (blue) as cell marker. Note that OCN first manifests as a punctate peri-nuclear stain (days 3, 10), then matures into a punctate cytoplasmic/extracellular matrix protein stain (days 10, 16, 32, depicted with arrows). Similarly, OPN appears diffuse or undetectable (see supplemental figure 4) on days 3, 10, and 16; then matures into a punctate cytoplasmic staining on day 32 comparable to the OCN appearance (arrows). Positive staining for these late stage protein markers at day 32 suggests that MC3T3-E1 cells growing for extended periods on TAMP scaffolds differentiate into mature, bone matrix-secreting osteoblasts.

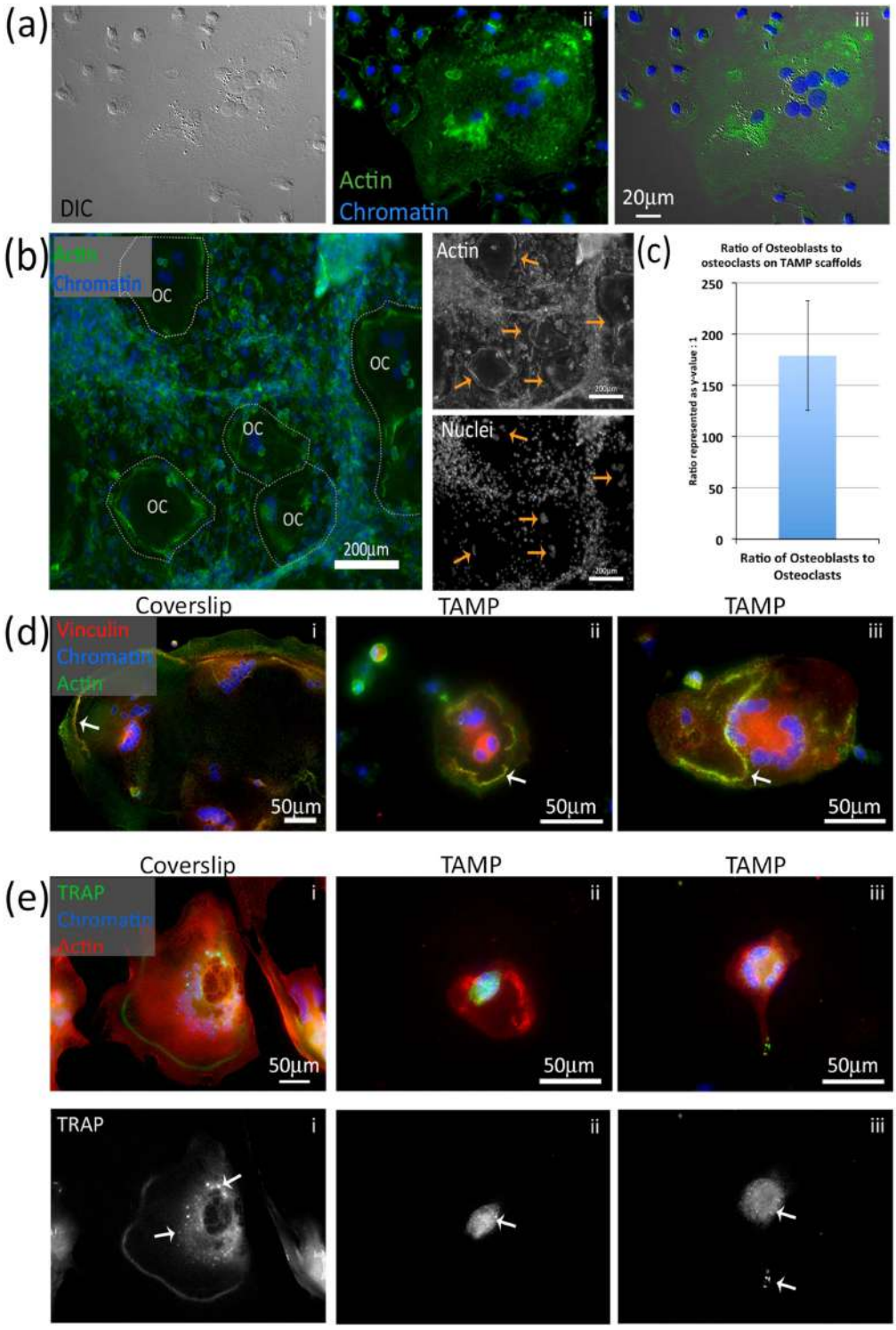

Figure 6. TAMP scaffolds promote the growth of co-cultured osteoblasts and osteoclasts into bone tissue-like arrangements. (a) To test the ability of TAMP scaffolds to support the growth of bone-like tissue, we isolated osteoclast precursor cells from rat femur bone marrow, differentiated them into mature osteoclasts, and seeded them together with MC3T3-E1 pre-osteoblasts onto glass coverslips and TAMP scaffolds. Osteoclasts with characteristic features (large cell size, multiple cell nuclei stained blue, large vesicular inclusions, and a sealing zone including actin protein stained green) were convincingly identifiable beside much smaller osteoblasts after 10 d of co-culture on cover slips in DIC white light and fluorescence images (panels i to iii). (b) Remarkably, 10 d of co-culture on TAMP scaffolds resulted in the formation of a complex, bone-like tissue structure that consisted of a dense network of MC3T3-E1 osteoblasts and interspersed osteoclasts (labeled with OC and outlined with dashed lines; actin-containing sealing zones and multi-nuclei clusters are labeled with arrows in the monochrome channel images on the right). (c) Quantitative analyses revealed a ratio of 179 $\pm$ 53 osteoblasts per osteoclasts, a ratio similar to human bone. (d) Co-staining actin (green), vinculin (red), and cell nuclei (blue) in osteoclasts growing on coverslips and TAMP scaffolds revealed a well-developed sealing zone (yellow, resulting color of merged green and red signals). (e) Staining osteoclasts for tartrate resistant acid phosphatase (TRAP) revealed expression of this enzyme, suggesting scaffold resorption (green, and depicted with arrows in the single-channel fluorescence images below).

chelators that gradually removes cells according to their size/adhesion strength, followed by staining remaining cells for actin, vinculin and chromatin (figure 6(c)). Treating TAMP scaffolds with Cell-stripper® removed the small-sized/less adherent osteoblasts, while large-sized/strongly adherent osteoclasts remained on the scaffolds. Vinculin (red) and actin (green) robustly co-localized in the sealing zones resulting in yellow, the overlay color of red and green as is typical for osteoclasts (figure 6(c), depicted with arrows).

Finally, to test whether osteoclasts are active when grown on TAMP scaffolds, we stained osteoclasts with antibodies specific for tartrate resistant acid phosphatase (TRAP). TRAP is an enzyme found in active osteoclasts that aids in the degradation of the bone matrix by dephosphorylating bone matrix phosphoproteins such as OPN and collagen [40–42]. In immunofluorescence images, TRAP (green) was detected as a diffuse as well as punctate, perinuclear stain (figure 6(d)). A similar staining pattern was observed on coverslips with TRAP being present in addition at the sealing zone of cells (figure 6(d), panel i). The positive TRAP staining of osteoclasts co-cultured on TAMP scaffolds correlated with the enzymatic detection of TRAP activity that was demonstrated using a colorimetric acid phosphatase kit (Sigma) that produces an insoluble red product. The presence of tartrate in the staining solution renders other acid phosphatases inactive making the stain specific to only TRAP positive cells [43–45]. A strong red staining of the co-cultured TAMP scaffold was detected, convincingly indicating robust TRAP enzyme activity (figure 7(a), panel 1 and quantified in (b)). No red product was detected on control scaffolds seeded with MC3T3-E1 cells only, or scaffolds not seeded with cells (figure 7(b), panels 2 and 3, B). Samples were counterstained with DAPI to verify the presence of cells on scaffolds (i) and (ii). No cells were detected on scaffold (iii) (figure 7(a), inserts, top left). Red color intensity was measured quantitatively using ImageJ software and supported the qualitative observation that the scaffolds with co-culture had active osteoclasts whereas scaffolds with only MC3T3-E1 cells or no cells did not. Taken together these analyses convincingly demonstrated that TAMP scaffolds support the growth of TRAP-producing osteoclasts suggesting active remodeling of TAMP scaffolds under osteoblast/osteoclast co-culture conditions, similarly to the dynamic remodeling of normal bone occurring *in situ*.

4. Discussion

Regenerating tissue using bioactive materials has many advantages over replacing it with inert, non-biological materials. 45S5 Bioglass® has been found to provide such bioactivity [1] and its application in, for example, bone regeneration is well established [2]. However, Bioglass® is a solid material and allows cells to bond to its surface only. Here, we demonstrate by performing a comprehensive biological characterization utilizing bone cells growing directly on as well as within the scaffolds, that next-generation TAMP silicates due to their high rate of interconnected macro and nano-porosity overcome these limitations. TAMP bio-scaffolds exhibit superior qualities for bone regeneration, which include cell bonding and penetration, cell differentiation, and scaffold remodeling by co-cultured osteoblasts and osteoclasts. Comprehensive SEM and immunofluorescence analyses show that MC3T3-E1 pre-osteoblast cells rapidly attach to TAMP scaffolds (within 1 h) and quickly spread out on the surface and inside the TAMP scaffolds. The formation of distinct actin stress fibers and robust focal adhesions are indicative of cells forming stable attachments to this stiff substrate [23, 25]. Cell proliferation analyses based on a quantitative Western blot-based assay revealed a cell-duplication time of approximately 3 d, somewhat slower than the 38 h reported by ATCC for these cells. As cell proliferation is known to be inversely coupled to cell differentiation [27, 46], a slower proliferation rate observed for MC3T3-E1 cells growing on/in TAMP scaffolds thus may support cell differentiation (as detailed below). Additionally, ions known to leach from TAMP and other sol-gel derived bioactive silicate glass materials have been found to be osteoinductive and to induce osteoblast precursor cells to differentiate [12–16], potentially further contributing to the differentiation of MC3T3-E1 growing on TAMP scaffolds. This is especially important to note since all experiments in this study were performed in the absence of osteogenic media.

As cell differentiation involves the specific up- and down-regulation of many different proteins, we performed quantitative mRNA-based RT-PCR analyses of MC3T3-E1 cells growing for 1, 7, 14, and 26 d on TAMP scaffolds. We found that integrins and growth factors were up-regulated early supporting our previous findings that MC3T3-E1 cells attached to, and proliferated on the TAMP scaffolds. These observations are consistent with an earlier study performed by Xynos *et al*, who reported that human osteoblasts treated with conditioned cell culture medium (medium exposed to bioactive glass for some time, consequently containing the ionic dissolution products of the glass material) exhibited up-regulation of proliferative factors and of other genes responsible for cell attachment [15]. Furthermore, we observed the up-regulation of distinct collagens, such as Collagen 1a1, indicating bone cell differentiation. MC3T3-E1 cell differentiation is further supported by the regulated expression of bone cell differentiation specific transcription factors. We found that Sox9 expression is high early, and drops as RunX2 expression increases. This is expected, since it is known that Sox9 expression must decrease to allow for RunX2 expression to increase and

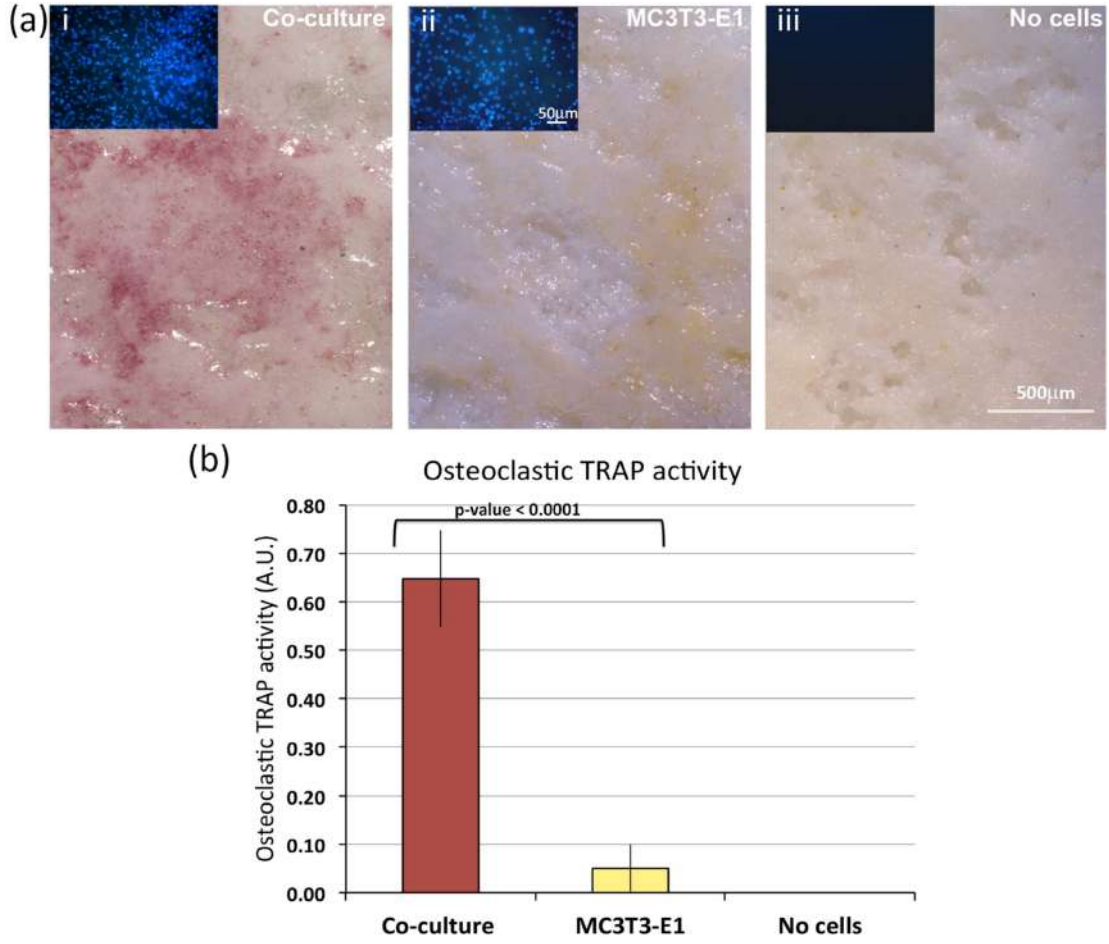

Figure 7. Osteoclasts cultured on TAMP scaffolds actively remodel the scaffolds. Osteoblasts together with osteoclasts, and osteoblasts alone were cultured on TAMP scaffolds, and TRAP activity was detected using a colorimetric acid phosphatase kit (Sigma). (a) Note red stain generated only in the presence of osteoclasts. To verify presence of cells on scaffolds i and ii, scaffolds were counter-stained with DAPI (insets, nuclei in blue). Scaffolds without cells showed no TRAP activity, nor DAPI stain (panel iii). (b) Quantitative analyses of 3-sets of scaffolds depicted in (a) revealed highly significant TRAP activity in the presence of osteoclastic cells.

differentiation to occur [47]. Gene expression of bone-specific secreted extracellular matrix proteins indicative of osteoblast differentiation (OPN and OCN) was up-regulated as well. These data are corroborated by studies done by others [12, 14, 15, 48], although several experimental differences are noteworthy including the use of cell types, time points of analyses, glass composition, and most importantly, the use of conditioned medium in other studies compared to growing cells directly on TAMP scaffolds.

Differentiation of MC3T3-E1 pre-osteoblasts when growing on TAMP scaffolds was further supported by analyses of differentiation markers on protein level. ALP enzyme activity was observed to continuously increase over time with a steeper increase towards longer time points (days 17, 21), correlating with observed reduced proliferation rates at these later times. Upregulation of ALP activity correlates with data reported by Christodoulou *et al*, who observed from days 7 to 14 a 4- to 8-fold increase in ALP activity of fetal osteoblasts exposed to low or high concentrations of bioactive glass conditioned medium, respectively [12]. OCN and OPN, proteins known to be secreted by mature osteoblasts into the extracellular calcified matrix [49–51] were detected by immunofluorescence staining as well. OCN was first detected as diffuse and perinuclear punctate labeling that later matured into larger, more distantly located puncta. These results are consistent with Filová *et al* who observed a punctate perinuclear stain of OCN in differentiating MG63 cells grown on hydroxyapatite [52]. Interestingly, punctate OPN was detected only at later time points (day 32) consistent with reports by others [53–55], who also detected OPN at late time points as a punctate Golgi-like stain. Taken together, our analyses strongly suggest MC3T3-E1 pre-osteoblastic cells differentiate into mature bone-producing osteoblasts when cultivated on TAMP scaffolds.

Bone not only consists of osteoblasts but also of several other cell types that interact to maintain its strength and health, as well as a sufficient amount of calcium in the blood [56]. Indeed, bone is remodeled continually; it is built by osteoblasts and degraded by osteoclasts (reviewed in [36, 57–59]). Osteoclasts generally have 3–20 cell nuclei generated by the fusion of precursor cells [60]. Typically, these cells are very

large, ranging from 100 to 200 μm in diameter (may be much larger *in vitro*) and characteristically form a sealing zone of actin and vinculin around the periphery of the cell [34, 36, 58, 59, 61]. This sealing zone provides a contained, low pH environment necessary for the activity of secreted enzymes that degrade the bone matrix. Osteoclasts are clearly distinguishable from other cells based on these unique morphological features.

To mimic the natural *in situ* environment, we co-cultured MC3T3-E1 pre-osteoblasts together with BMD hematopoietic stem cells that we isolated and differentiated *in vitro* resulting in a ratio of 179 $\pm$ 53 osteoblasts per osteoclast, similar to ratios reported in humans [39]. Remarkably, the co-cultured osteoblastic and osteoclastic cells (identifiable by the features described) formed a complex tissue-like structure when cultured on TAMP scaffolds. In order to degrade calcified bone structure, osteoclasts produce specific enzymes, e.g. TRAP, that are secreted into the resorption lacunae, a compartment formed basally between the bone surface, sealing zone, and ruffled boarder (a specialized invaginated membrane that resembles late endosomal membrane that serves to secrete substances required for degradation and resorption of the bone matrix) [62, 63]. Once proteins have been degraded, they are resorbed into the osteoclasts and follow a transcytotic pathway until they are secreted into the extracellular space at the apical side of the cell. TRAP has been described to be secreted, but to also localize to these transcytotic vesicles to further enhance collagen degradation before secretion to the extracellular space [34, 64]. Using immunofluorescence detection of TRAP, these vesicles were observed in osteoclasts co-cultured on TAMP scaffolds. Our findings are consistent with results by others [65–68] who showed that osteoclasts degraded hydroxyapatite *in vitro*. TRAP biosynthesis and secretion indicates that the osteoclasts actively degraded TAMP scaffold matrix, while osteoblasts secreted bone matrix, suggesting active remodeling of the scaffold material.

5. Conclusions

Here we show that MC3T3-E1 pre-osteoblasts attach, proliferate and differentiate into mature, calcified matrix secreting osteoblasts, and BMD cells differentiate into active, TRAP secreting osteoclasts when cultured on TAMP calcium silicate scaffolds, indicating that this bioactive glass material can support the dynamic remodeling activities that are required for successful bone growth and repair. Our *in vitro* results are supported by results obtained *in situ* using subcutaneous rabbit skin and human mandible implant studies [3, 7]. As TAMP scaffold chemistry and porosity are easily 'tailored', modifications in the chemical composition promise that TAMP scaffolds will meet the many challenging specifics of various bone regeneration applications.

Acknowledgments

The authors acknowledge the National Science Foundation for supporting this work via International Materials Institute for New Functionality in Glass (IMI-NFG, DMR-0844014) and PFI:AIR-TT (IIP-1602057) programs, repeated Howard Hughes Medical Institute funded Biosystems Dynamics Summer Institute (HHMI-BDSI) grants, an Innovators' Circle grant from the Abington Health Foundation, and NIH to support work in the laboratory of MMF (NIH-NIGMS, grant R01 GM55725).

Disclosure statement

The authors declare that no competing financial interests exist.

Author contributions

TJK designed and performed experiments, evaluated data, wrote the draft manuscript, generated figures and edited the manuscript; NCH performed experiments and evaluated data, edited the manuscript; SE performed experiments and evaluated data; JYM designed experiments, helped performing experiments and analyzed data; DMF performed experiments; UT helped to design experiments and evaluate data; HJ designed experiments, evaluated data and edited the manuscript; MMF designed experiments, supervised research, evaluated data and edited the manuscript.

ORCID iDs

Tia J Kowal https://orcid.org/0000-0003-3879-4718
Daniella M Fodera https://orcid.org/0000-0002-6162-8761

References

[1] Hench L 2006 The story of Bioglass *J. Mater. Sci., Mater. Med.* **17** 967–78
[2] Jones J R 2013 Review of bioactive glass: from hench to hybrids *Acta Biomater.* **9** 4457–86
[3] El Shazley N *et al* 2016 Bioglass in alveolar bone regeneration in orthodontic patients randomized controlled clinical trial *JDR Clin. Transl. Res.* **1** 244–55
[4] Marques A, Almeida R, Thiema A, Wang S, Falk M and Jain H 2009 Sol-gel derived glass scaffold with high pore interconnectivity and enhanced bioactivity *J. Mater. Res.* **24** 34953502
[5] Vueva Y *et al* 2010 Monolithic glass scaffolds with dual porosity prepared by polymer-induced phase separation and sol-gel *J. Am. Ceram. Soc.* **93** 1945–9

[6] Wang S *et al* 2011 Evaluation of 3D nano-macro porous bioactive glass scaffold for hard tissue engineering *J. Mater. Sci. Mater. Med.* **22** 1195–203
[7] Wang S, Kowal T, Marei M, Falk M and Jain J 2013 Nanoporosity significantly enhances the biological performance of engineered glass tissue scaffolds *Tissue Eng.* A **19** 1632–40
[8] Zhang D, Jain H, Hupa M and Hupa L 2012 *In-vitro* degradation and bioactivity of tailored amorphous multi porous scaffold structure *J. Am. Ceram. Soc.* **95** 2687–94
[9] Baino F and Ferraris M 2017 Learning from nature: using bioinspired approaches and natural materials to make porous bioceramics *Int. J. Appl. Ceram. Technol.* **14** 507–20
[10] Baino F, Fiorilli S and Vitale-Brovarone C 2016 Bioactive glass-based materials with hierarchical porosity for medical applications: review of recent advances *Acta Biomater.* **42** 18–32
[11] Chung J J, Li S, Stevens M M, Georgiou T K and Jones J 2016 Tailoring mechanical properties of sol-gel hybrids for bone regeneration through polymer structure *Chem. Mater.* **28** 6127–35
[12] Christodoulou I, Buttery L D, Saravanapavan P, Tai G, Hench L L and Polak J M 2005 Dose-and time-dependent effect of bioactive gel-glass ionic-dissolution products on human fetal osteoblast-specific gene expression *J. Biomed. Mater. Res.* B **74** 529–37
[13] Gough J E, Jones J R and Hench L L 2004 Nodule formation and mineralisation of human primary osteoblasts cultured on a porous bioactive glass scaffold *Biomaterials* **25** 2039–46
[14] Jones J R, Tsigkou O, Coates E E, Stevens M M, Polak J M and Hench L L 2007 Extracellular matrix formation and mineralization on a phosphate-free porous bioactive glass scaffold using primary human osteoblast (HOB) cells *Biomaterials* **28** 1653–63
[15] Xynos I D, Edgar A J, Buttery L D, Hench L L and Polak J M 2001 Gene-expression profiling of human osteoblasts following treatment with the ionic products of Bioglass® 45S5 dissolution *J. Biomed. Mater. Res.* A **55** 151–7
[16] Tsigkou O, Jones J R, Polak J M and Stevens M M 2009 Differentiation of fetal osteoblasts and formation of mineralized bone nodules by 45S5 Bioglass® conditioned medium in the absence of osteogenic supplements *Biomaterials* **30** 3542–50
[17] Brunauer S, Emmett P H and Teller E 1938 Adsorption of gases in multimolecular layers *J. Am. Chem. Soc.* **60** 309–19
[18] Midha S, Kim T B, van den Bergh W, Lee P D, Jones J R and Mitchell C A 2013 Preconditioned 70S30C bioactive glass foams promote osteogenesis *in vivo Acta Biomater.* **9** 9169–82
[19] Dobson K R, Reading L, Haberey M, Marine X and Scutt A 1999 Centrifugal isolation of bone marrow from bone: an improved method for the recovery and quantitation of bone marrow osteoprogenitor cells from rat tibiae and femurae *Calcified Tissue Int.* **65** 411–3
[20] Tanaka S *et al* 1993 Macrophage colony-stimulating factor is indispensable for both proliferation and differentiation of osteoclast progenitors *J. Clin. Invest.* **91** 257
[21] Boccaccini A R, Brauer D S and Hupa L 2016 *Bioactive Glasses: Fundamentals, Technology and Applications* vol 23 (London: Royal Society of Chemistry)
[22] Herman B and Pledger W J 1985 Platelet-derived growth factor-induced alterations in vinculin and actin distribution in BALB/c-3T3 cells *J. Cell Biol.* **100** 1031–40
[23] Discher D E, Janmey P A and Wang Y 2005 Tissue cells feel and respond to the stiffness of their substrate *Science* **310** 1139–43
[24] Solon J, Levental I, Sengupta K, Georges P C and Janmey P A 2007 Fibroblast adaptation and stiffness matching to soft elastic substrates *Biophys. J.* **93** 4453–61
[25] Yeung T *et al* 2005 Effects of substrate stiffness on cell morphology, cytoskeletal structure, and adhesion *Cell Motil. Cytoskeleton* **60** 24–34
[26] Robinson M S 1989 Cloning of cDNAs encoding two related 100 kD coated vesicle proteins (a-adaptins) *J. Cell Biol.* **108** 3
[27] Sudo H, Kodama H, Amagai Y, Yamamoto S and Kasai S 1983 *In vitro* differentiation and calcification in a new clonal osteogenic cell line derived from newborn mouse calvaria *J. Cell Biol.* **96** 191–8
[28] Quarles L D, Yohay D A, Lever L W, Caton R and Wenstrup R J 1992 Distinct proliferative and differentiated stages of murine MC3T3-E1 cells in culture: an *in vitro* model of osteoblast development *J. Bone Miner. Res.* **7** 683–92
[29] Choi J *et al* 1996 Expression patterns of bone-related proteins during osteoblastic differentiation in MC3T3-E1 cells *J. Cell. Biochem.* **61** 609–18
[30] Russell R G, Mühlbauer R C, Bisaz S, Williams D A and Fleisch H 1970 The influence of pyrophosphate, condensed phosphates, phosphonates and other phosphate compounds on the dissolution of hydroxyapatite*in vitro* and on bone resorption induced by parathyroid hormone in tissue culture and in thyroparathyroidectomised rats *Calcified Tissue Int.* **6** 183–96
[31] Felix R and Fleisch H 1979 Increase in alkaline phosphatase activity in calvaria cells cultured with diphosphonates *Biochem. J.* **183** 73–81
[32] Owen T A *et al* 1990 Progressive development of the rat osteoblast phenotype *in vitro*: reciprocal relationships in expression of genes associated with osteoblast proliferation and differentiation during formation of the bone extracellular matrix *J. Cell. Physiol.* **143** 420–30
[33] Robling A G, Castillo A B and Turner C H 2006 Biomechanical and molecular regulation of bone remodeling *Annu. Rev. Biomed. Eng.* **8** 455–98
[34] Väänänen H K, Zhao H, Mulari M and Halleen J M 2000 The cell biology of osteoclast function *J. Cell Sci.* **113** 377–81
[35] Teitelbaum S L 2000 Bone resorption by osteoclasts *Science* **289** 1504–8
[36] Soysa N S, Neil A, Aoki K and Ohya K 2012 Osteoclast formation and differentiation: an overview *J. Med. Dental Sci.* **59** 65–74
[37] Jimi E *et al* 1996 Osteoclast function is activated by osteoblastic cells through a mechanism involving cell-to-cell contact *Endocrinology* **137** 2187–90
[38] Coetzee M, Haag M and Kruger M C 2007 Effects of arachidonic acid, docosahexaenoic acid, prostaglandin E2 and parathyroid hormone on osteoprotegerin and RANKL secretion by MC3T3-E1 osteoblast-like cells *J. Nutritional Biochem.* **18** 54–63
[39] Gruber H E, Ivey J L, Thompson E R, Chesnut C H and Baylink D J 1985 Osteoblast and osteoclast cell number and cell activity in postmenopausal osteoporosis *Miner. Electrolyte Metab.* **12** 246–54
[40] Minkin C 1982 Bone acid phosphatase: tartrate-resistant acid phosphatase as a marker of osteoclast function *Calcified Tissue Int.* **34** 285–90
[41] Hollberg K, Hultenby K, Hayman A R, Cox T M and Andersson G 2002 Osteoclasts from mice deficient in tartrate-resistant acid phosphatase have altered ruffled borders and disturbed intracellular vesicular transport *Exp. Cell Res.* **279** 227–38
[42] Suter A *et al* 2001 Overlapping functions of lysosomal acid phosphatase (LAP) and tartrate-resistant acid phosphatase (Acp5) revealed by doubly deficient mice *Development* **128** 4899–910
[43] Fishman W H, Dart R M, Bonner C D, Leadbetter W F, Lerner F and Homburger F 1953 A new method for estimating serum acid phosphatase of prostatic origin applied to the clinical investigation of cancer of the prostate *J. Clin. Invest.* **32** 1034
[44] Roy A V, Brower M E and Hayden J E 1971 Sodium thymolphthalein monophosphate: a new acid phosphatase substrate with greater specificity for the prostatic enzyme in serum *Clin. Chem.* **17** 1093–102
[45] LaCount M W, Handy G and Lebioda L 1998 Structural origins of L (+)-tartrate inhibition of human prostatic acid phosphatase *J. Biol. Chem.* **273** 30406–9

[46] Kodama H, Amagai Y, Sudo H, Kasai S and Yamamoto S 1981 Establishment of a clonal osteogenic cell line from newborn mouse calvaria *Japan. J. Oral Biol.* **23** 899–901
[47] Wang Y and Sul H S 2009 Pref-1 regulates mesenchymal cell commitment and differentiation through Sox9 *Cell Metab.* **9** 287–302
[48] Varanasi V G *et al* 2009 Enhanced osteocalcin expression by osteoblast-like cells (MC3T3-E1) exposed to bioactive coating glass (SiO2–CaO–P2O5–MgO–K2O–Na2O system) ions *Acta Biomater.* **5** 3536–47
[49] Franzen A and Heinegård D 1985 Isolation and characterization of two sialoproteins present only in bone calcified matrix *Biochem. J.* **232** 715–24
[50] Hauschka P V, Lian J B and Gallop P M 1975 Direct identification of the calcium-binding amino acid, gamma-carboxyglutamate, in mineralized tissue *Proc. Natl Acad. Sci.* **72** 3925–9
[51] Price P A, Otsuka A A, Poser J W, Kristaponis J and Raman N 1976 Characterization of a gamma-carboxyglutamic acid-containing protein from bone *Proc. Natl Acad. Sci.* **73** 1447–51
[52] Filová E *et al* 2014 Support for the initial attachment, growth and differentiation of MG-63 cells: a comparison between nano-size hydroxyapatite and micro-size hydroxyapatite in composites *Int. J. Nanomed.* **9** 3687
[53] Tsutsumi K, Saito N, Kawazoe Y, Ooi H and Shiba T 2014 Morphogenetic study on the maturation of osteoblastic cell as induced by inorganic polyphosphate *PLoS One* **9** e86834
[54] Ruckh T T, Carroll D A, Weaver J R and Popat K C 2012 Mineralization content alters osteogenic responses of bone marrow stromal cells on hydroxyapatite/polycaprolactone composite nanofiber scaffolds *J. Funct. Biomater.* **3** 776–98
[55] Przybylowski C *et al* 2012 MC3T3 preosteoblast differentiation on bone morphogenetic protein-2 peptide ormosils *J. Mater. Chem.* **22** 10672–83
[56] Bronner F 1991 Bone and calcium homeostasis *Neurotoxicology* **13** 775–82
[57] Väänänen H K and Laitala-Leinonen T 2008 Osteoclast lineage and function *Arch. Biochem. Biophys.* **473** 132–8
[58] Linkhart T A *et al* 1999 Osteoclast formation in bone marrow cultures from two inbred strains of mice with different bone densities *J. Bone Miner. Res.* **14** 39–46
[59] Blair H C 1998 How the osteoclast degrades bone *Bioessays* **20** 837–46
[60] Suda T, Takahashi N and Martin T J 1992 Modulation of osteoclast differentiation *Endocrine Rev.* **13** 66–80
[61] Väänänen H K and Horton M 1995 The osteoclast clear zone is a specialized cell-extracellular matrix adhesion structure *J. Cell Sci.* **108** 2729–32
[62] Blair H C, Teitelbaum S L, Ghiselli R and Gluck S 1989 Osteoclastic bone resorption by a polarized vacuolar proton pump *Science* **245** 855–8
[63] Salo J, Metsikko K, Palokangas H, Lehenkari P and Vaananen H K 1996 Bone-resorbing osteoclasts reveal a dynamic division of basal plasma membrane into two different domains *J. Cell Sci.* **109** 301–7
[64] Halleen J M *et al* 1999 Intracellular fragmentation of bone resorption products by reactive oxygen species generated by osteoclastic tartrate-resistant acid phosphatase *J. Biol. Chem.* **274** 22907–10
[65] Yamada S, Heymann D, Bouler J M and Daculsi G 1997 Osteoclastic resorption of biphasic calcium phosphate ceramic *in vitro J. Biomed. Mater. Res.* **37** 346–52
[66] Monchau F, Lefevre A, Descamps M, Belquin-Myrdycz A, Laffargue P and Hildebrand H F 2002 *In vitro* studies of human and rat osteoclast activity on hydroxyapatite, β-tricalcium phosphate, calcium carbonate *Biomol. Eng.* **19** 143–52
[67] Detsch R, Mayr H and Ziegler G 2008 Formation of osteoclast-like cells on HA and TCP ceramics *Acta Biomater.* **4** 139–48
[68] Midha S, van den Bergh W, Kim T B, Lee P D, Jones J R and Mitchell C A 2013 Bioactive glass foam scaffolds are remodelled by osteoclasts and support the formation of mineralized matrix and vascular networks *in vitro Adv. Healthcare Mater.* **2** 490–9